

Article

Finite Element Analysis of Strengthening Mechanism of Ultrastrong and Tough Cellulosic Materials

Xiaoshuai Han ¹, Jingwen Wang ¹, Xiaoyi Wang ¹, Wei Tian ¹, Yanyan Dong ^{2,*} and Shaohua Jiang ^{1,*} 

¹ Jiangsu Co-Innovation Center of Efficient Processing and Utilization of Forest Resources, International Innovation Center for Forest Chemicals and Materials, College of Materials Science and Engineering, Nanjing Forestry University, Nanjing 210037, China

² Institute of Environment and Sustainable Development in Agriculture, Chinese Academy of Agricultural Sciences, Beijing 100081, China

* Correspondence: dongyanyan@caas.cn (Y.D.); shaohua.jiang@njfu.edu.cn (S.J.);
Tel.: +86-173-0121-7475 (Y.D.); +86-025-85428090 (S.J.)

Abstract: Superior strong and tough structural materials are highly desirable in engineering applications. However, it remains a big challenge to combine these two mutually exclusive mechanical properties into one body. In the work, an ultrastrong and tough cellulosic material was fabricated by a two-step process of delignification and water molecule-induced hydrogen bonding under compression. The strong and tough cellulosic material showed enhanced tensile strength (352 MPa vs. 56 MPa for natural wood) and toughness (4.1 MJ m⁻³ vs. 0.42 MJ m⁻³ for natural wood). The mechanical behaviors of ultrastrong and tough bulk material in a tensile state were simulated by finite element analysis (FEA) using mechanical parameters measured in the experiment. FEA results showed that the tensile strength and toughness gradually simultaneously improved with the increase in moisture content, demonstrating that water molecules played an active role in fabricating strong and tough materials, by plasticizing and forming hydrogen bonding among cellulose nanofibrils.



Citation: Han, X.; Wang, J.; Wang, X.; Tian, W.; Dong, Y.; Jiang, S. Finite Element Analysis of Strengthening Mechanism of Ultrastrong and Tough Cellulosic Materials. *Polymers* **2022**, *14*, 4490. <https://doi.org/10.3390/polym14214490>

Academic Editor: Jem-Kun Chen

Received: 30 September 2022

Accepted: 22 October 2022

Published: 24 October 2022

Publisher's Note: MDPI stays neutral with regard to jurisdictional claims in published maps and institutional affiliations.



Copyright: © 2022 by the authors. Licensee MDPI, Basel, Switzerland. This article is an open access article distributed under the terms and conditions of the Creative Commons Attribution (CC BY) license (<https://creativecommons.org/licenses/by/4.0/>).

Keywords: wood; cellulose nanofibril; hydrogen bonding; strengthening; finite element analysis (FEA)

1. Introduction

High-performance structural materials with high strength and fracture toughness have consistently drawn significant attention and are in great demand in the modern manufacturing industry [1–6]. When developing such high-strength and tough structural materials, natural polymers should be preferred due to their renewable and sustainable characteristics [7,8]. Cellulose is the most abundant biopolymer on Earth, found in trees, bamboo, rattan, agricultural crops, and other biomass, even bacteria [9–14]. Cellulose possesses attractive intrinsic mechanical properties with tensile strength of about 3.0–4.7 GPa g⁻¹ cm³ and a theoretical modulus of about 63–125 GPa g⁻¹ cm³ in its crystal region [15,16], both of which are higher than most metals, alloys, and some ceramics, which makes it an ideal building block for a series of strong and tough materials, such as nanopaper, films, and superstrong wood [17–19].

In general, cellulose-derived materials (cellulose nanofibrils or cellulose crystals) could be directly bought from a factory and corresponding structural materials can be fabricated using bottom-up assembly methods such as vacuum filtration, layer-by-layer assembly, or solvent casting [20–24]. However, this bottom-up assembly method has some intrinsic drawbacks including (1) cellulose-derived materials' isolation is chemical–energy intensive; (2) the assembly process is time-consuming and laborious and complicated; (3) the products are usually on a small scale and hard to transfer to bulk materials. Recently, a top-down recombination method has been adapted to fabricate large-scale cellulosic structural materials due to their natural disadvantages of aligned nanocellulose structure [25–30]. During the fabrication process, some kinds of organic (epoxy, phenolic resin, etc.) or inorganic

polymers (nanosilica, calcium carbonate, etc.) were combined with a cellulosic framework to improve the physical and mechanical properties of products [31–33]. Our group also proposed a simple yet universal top-down method for making strong and tough structural materials by water molecule-induced hydrogen bonding. This method can convert natural wood into strong and tough bulk materials by a three-step process of delignification, drying-induced assembly, and water molecule-induced hydrogen bonding under compression. A tough and strong cellulose nanofiber bulk material was derived, showing simultaneously enhanced tensile strength (352 MPa vs. 56 MPa for natural wood) and toughness (4.1 MJ m^{-3} vs. 0.42 MJ m^{-3} for natural wood) [34]. Although we analyzed the plasticizing and strengthening mechanism of water molecules for cellulose nanofibrils, this explanation can only be indirectly characterized by macroscopic physical and mechanical data. Some visible means of characterization is necessary for identifying the water molecule-induced strengthening mechanism between cellulose nanofibrils. Finite element analysis (FEA) has been commonly used in engineering fields by virtue of developing technologies [35,36]. Meanwhile, FEA has also been confirmed as an effective method commonly used in wood engineering [37,38].

In this study, a methodological means was proposed: the water molecule-induced hydrogen bonding effect between cellulose nanofibrils was investigated numerically by first using FEA. The relationship between hydrogen bonding and tensile properties was analyzed by comparing FEA simulation and experimental data.

2. Materials and Methods

2.1. Materials and Chemicals

Basswood with dimensions of 50 mm (L) \times 50 mm (T) \times 10 mm (R) was used in this study. Sodium chlorite (NaClO_2 , 80%), sulfuric acid (H_2SO_4 , 72%), acetic acid (HAc, 99.7%), potassium sulfate (K_2SO_4), acetone (99.8%), and hexane (99.8%) were purchased from Fisher Scientific (Thermo Fisher Scientific Inc., Shanghai, China). All chemicals were used as received without further purification. Deionized (DI) water was used for sample preparation.

2.2. Fabrication of Ultrastrong and Tough Cellulose Nanofibril Bulk Material

Basswood was chemically treated to remove most lignin and partial hemicellulose and then dried using a solvent exchange drying method, followed by compression to the final ultrastrong and tough cellulose nanofibril bulk material according to a previous report [34]. In this study, NW stands for natural basswood, DW stands for delignified wood, DW_{SD} stands for delignified wood by solvent exchange drying, CDW_{SD} stands for compressed delignified wood by solvent exchange drying, followed by drying at 105 °C; $\text{CDW}_{\text{SD}0}$ stands for compressed delignified wood under 0% moisture content, followed by drying at 105 °C; $\text{CDW}_{\text{SD}9}$ stands for compressed delignified wood under 9% moisture content, followed by drying at 105 °C; $\text{CDW}_{\text{SD}18}$ stands for compressed delignified wood under 18% moisture content, followed by drying at 105 °C.

2.3. Characterization

The chemical compositions of both natural wood (NW) and delignified wood (DW) were qualitatively analyzed by a Nicolet 6700 infrared spectrophotometer (IR, Thermo Scientific, Waltham, MA, USA) equipped with an ATR accessory. The lignin contents (Klason lignin) of NW and DW were determined according to a standard TAPPI T 222 om-2 method [39]. The morphologies of NW, DW, compressed delignified wood by solvent exchange drying compressed under 0% moisture content ($\text{CDW}_{\text{SD}0}$), 9% moisture content ($\text{CDW}_{\text{SD}9}$), and 18% moisture content ($\text{CDW}_{\text{SD}18}$) were characterized using a Phenom XL G2 Desktop scanning electron microscope. The mechanical properties of the samples were measured using an Academic User Instron 5969 Uniaxial Materials Testing System (Instron 5969, Norwood, MA, USA). At least ten specimens were tested for all samples and the averages and standard deviations were presented.

The densities of NW, DW_{SD}, CDW_{SD0}, CDW_{SD9}, and CDW_{SD18} were determined from the ratios of mass to volume. The porosities of the above samples were calculated as follows:

$$\text{Porosity (\%)} = \left(1 - \frac{\rho_a}{\rho_b}\right) \times 100\%$$

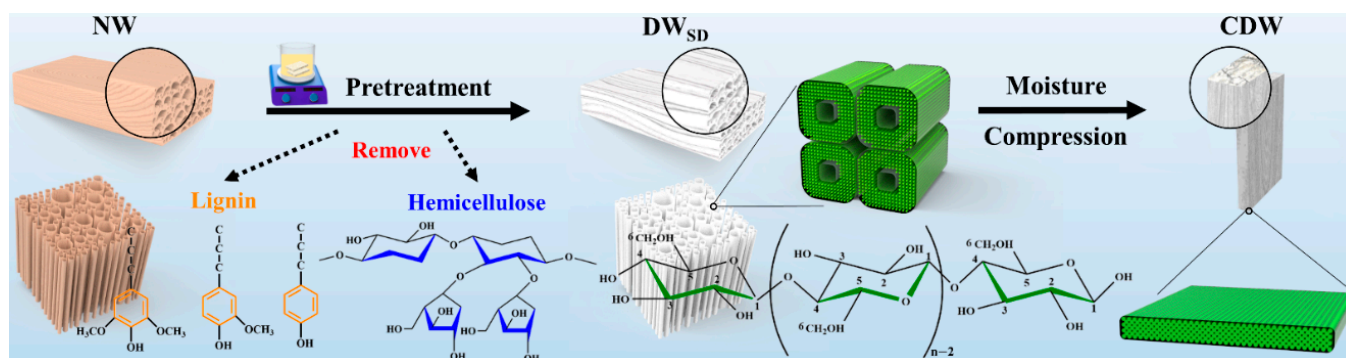
where ρ_a is the density of the cellulose nanofiber bulk material and ρ_b is the density of the delignified wood, taken as 1.5 g·cm⁻³.

2.4. Numerical Modeling of Ultrastrong and Tough Bulk Material

The fabricated ultrastrong and tough bulk material is simulated for validation of the model for strength, stiffness, and failure mechanisms by macro and micro finite element analysis (FEA). The macro FEA of the tension test based on a 3D solid model was performed. The micro FEA construction of tension test included two steps: (1) the length of cellulose nanofibril was assumed to be 7.5 μm and the transverse section's side length was 3.5 nm. The vertical distances between cellulose nanofibrils were 0.29 nm (0% moisture content), 0.17 nm (9% moisture content), and 0.13 nm (18% moisture content), respectively. The distance along the cellulose nanofibrils' ends was assumed to be 0.5 nm. After that, finite element software ABAQUS (ABAQUS version 2014) was used to capture representative bulk unit cells consisting of wood cellulose nanofibrils and mesenchyme. Figure S1 (Supporting Information) shows representative bulk unit cell models of CDW_{SD0}, CDW_{SD9}, and CDW_{SD18}; (2) determination of the conditions for FEA. Based on the representative bulk unit cell model above, the conditions of micro FEA were determined as follows: the fracture strength and Young's modulus of microfibrils were set as 2.3 GPa and 129 GPa, respectively [10,40]. The strength of nanofibril mesenchyme was unknown and it represented the bonding force between cellulose nanofibrils under different moisture contents. The mechanical properties of mesenchyme were characterized through simulating and comparing the experimental tensile strength and fracture strain data, which revealed bonding force between cellulose nanofibrils of CDW_{SD0}, CDW_{SD9}, and CDW_{SD18}.

3. Results

Scheme 1 shows our top-down approach for fabricating ultrastrong and tough cellulose nanofibril bulk material with the aid of water molecule-induced hydrogen bonding. In detail, this material was fabricated following a three-step process: (1) delignification to remove hydrophobic lignin and ionic interacted hemicellulose, which exposed well-aligned cellulose nanofibrils and enhanced hydrogen bonding ability; (2) a solvent exchange drying method was employed to remove water and maintain the original wooden framework facilitating water molecule adsorption; (3) rehydration of solvent exchange dried delignified wood to different moisture content levels, followed by mechanical compression to introduce hydrogen bonding for enhanced mechanical performance.



Scheme 1. Schematic illustration of the top-down fabrication of ultrastrong and tough cellulose nanofibril bulk material with delignification, solvent exchange drying, moisture absorption, and compression process.

In order to investigate the water molecule-induced hydrogen bonding effect on intercellulose nanofibrils, the natural basswood was subjected to sodium chlorite (NaClO_2) and sodium hydroxide (NaOH) treatment to remove lignin and hemicellulose. The result showed that the DW sample was composed of 80.2% cellulose, 14.7% hemicellulose, and 2.1% lignin, indicating 22% hemicellulose and 91% lignin removal (Figure 1a). The delignification result was further validated by FTIR spectroscopy (Figure 1b). There are typical hemicellulose absorption peaks at 1734 cm^{-1} (unconjugated carbonyl $\text{C}=\text{O}$) and lignin absorption peaks at 1507 cm^{-1} and 1595 cm^{-1} ($\text{C}=\text{H}$ stretching of the aromatic rings), 1365 cm^{-1} (symmetric $\text{C}-\text{H}$ bending from methoxyl group), and 1234 cm^{-1} ($\text{C}-\text{O}$ stretching of the aromatic rings) in natural basswood. However, the above absorption peaks disappeared in DW after NaClO_2 and NaOH treatment. As the hemicellulose and lignin were removed, the DW_{SD} had lower density (0.21 g cm^{-3}) and higher porosity (86.00%) compared to natural basswood. In order to validate the water molecule-induced hydrogen bonding strengthening effect, the DW_{SD} absorbed different water vapor contents (0% moisture content, 9% moisture content, and 18% moisture content) and was then compressed and dried. The result presented that the density of CDW_{SD} increased and the porosity decreased with increasing moisture content, indicating a positive effect of water molecules for improving the densification degree of the cellulose nanofibrils within DW_{SD} (Figure 1c,d).

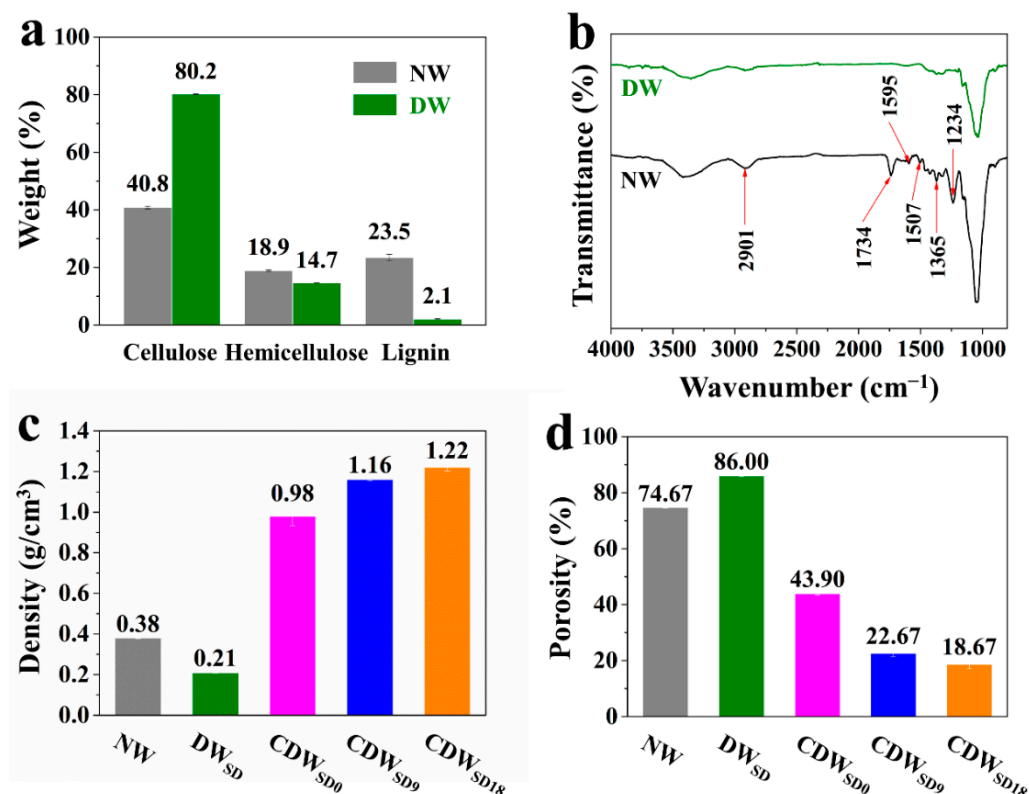


Figure 1. (a) The composition of cellulose, hemicellulose, and lignin in natural wood (NW) and delignified wood (DW). (b) FTIR spectra of NW and DW. (c) Density and (d) porosity of NW, delignified wood by solvent exchange drying (DW_{SD}), compressed delignified wood by solvent exchange drying compressed under 0% moisture content ($\text{CDW}_{\text{SD}0}$), 9% moisture content ($\text{CDW}_{\text{SD}9}$), and 18 moisture content ($\text{CDW}_{\text{SD}18}$).

The morphologies of NW, DW_{SD} , $\text{CDW}_{\text{SD}0}$, $\text{CDW}_{\text{SD}9}$, and $\text{CDW}_{\text{SD}18}$ are presented in Figures 2 and S2 (Supporting Information). Compared with NW, the volume of DW_{SD} was slightly reduced (Figure 2a), indicating that the solvent exchange drying technique did not destroy the microstructure of NW. The SEM cross-section images of NW and DW_{SD} (Figure 2b,c) showed the separated individual wood cells, showing non-polar hexane restricted the association between wood fibers. In addition, the wood cell walls of DW_{SD}

was thinner than that of NW because of hemicellulose and lignin removal. As we all know, DW is a hygroscopic material, which tends to bind water molecules through hydrogen bonding via its surface hydroxyl groups. In order to investigate the effect of bound water on the densification and mechanical properties of the delignified wood, the DW_{SD} absorbed a given mass of moisture (0%, 9%, and 18%) in a desiccator containing K_2SO_4 solution, which can provide $97.6 \pm 0.5\%$ relative humidity (RH) at $20^\circ C$. The DW_{SD} having different moisture contents were then compressed and dried. At 0% moisture content, the DW_{SD} could not be compressed to a dense material and the CDW_{SD0} experienced springback, indicating cellulose nanofibrils could not tightly link together. Therefore, there are a lot of big gaps caused by fewer bindings among wood cells (Figure 2d). When increasing moisture content on the surface of cellulose nanofibers, the CDW_{SD} showed more dense and compact cross-section microstructure, which is because water molecules can be plasticizers, increasing the flexibility and softness of cellulose nanofibers and causing wood cell walls to tightly intertwine and densely pack together under compression. Additionally, more bound water molecules on the surface of cellulose nanofibers increased the hydrogen bonding capacity, creating more strong interactions between cellulose nanofibrils. Thus, these big gaps disappeared and there were fewer microcracks in the CDW_{SD9} (Figure 2e). For CDW_{SD18} , the cellulose nanofibrils inside cell walls had merged together by compression (Figure 2f). The above results were also consistent with the density and porosity analyses as shown in Figure 1c,d.

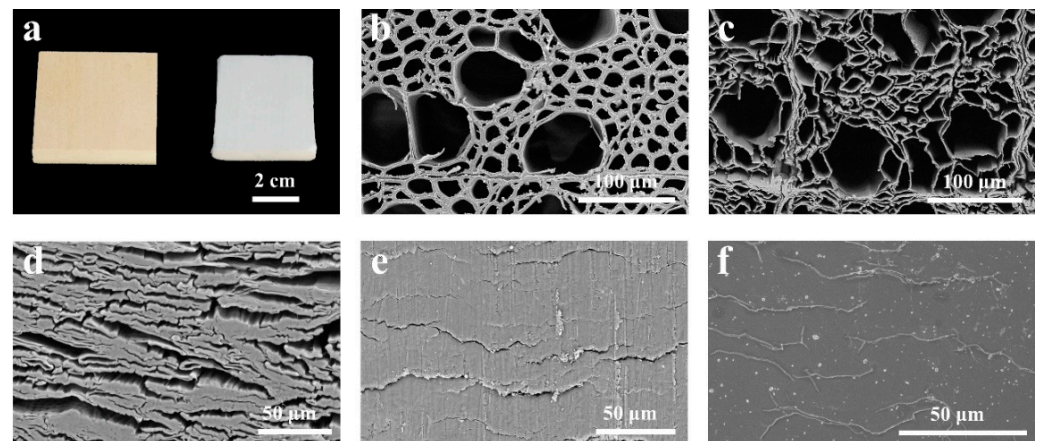


Figure 2. (a) Photographs of NW and DW_{SD} . SEM cross-section images of (b) NW, (c) DW_{SD} , (d) CDW_{SD0} , (e) CDW_{SD9} , and (f) CDW_{SD18} .

Figure 3 demonstrates tensile–strain curves and the corresponding mechanical performance of the NW, DW_{SD} , CDW_{SD0} , CDW_{SD9} , and CDW_{SD18} . Due to the loose and separated structure formed during delignification and solvent exchange drying, the DW_{SD} showed low mechanical properties with tensile strength, Young’s modulus, and toughness of 43.4 MPa, 5.5 GPa, and 0.4 MJ m^{-3} , respectively, which were lower than those of NW (55.8 MPa, 6.0 GPa, and 0.4 MJ m^{-3}). For compressed solvent exchange dried delignified wood, the mechanical properties increased with increasing moisture content prior to compression. The tensile strength (351.8 MPa), Young’s modulus (32.9 GPa), and toughness (4.1 MJ m^{-3}) of CDW_{SD18} were more than 5, 3, and 6 times higher than those of CDW_{SD0} . As previously discussed, the CDW_{SD0} displayed a springback phenomenon and big gap microstructure due to mutually exclusive hydroxide groups, which could not form enough hydrogen bonds when compressed at 0% moisture content. The mechanical performance change clearly indicated that water molecules played the role of plasticizers and structural molecules between cellulose nanofibrils to enhance the hydrogen bonding interactions of inter-nanofibrils.

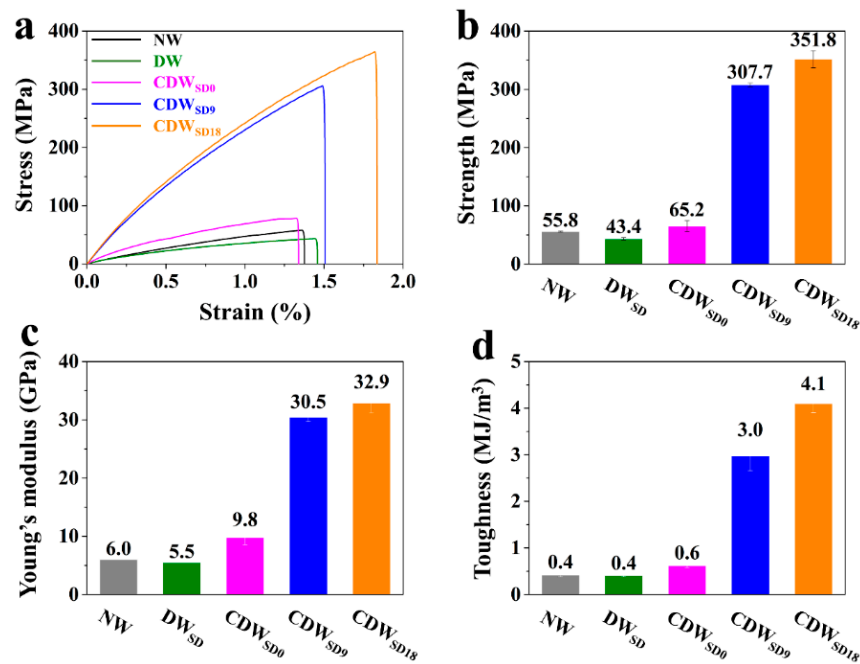


Figure 3. (a) Typical tensile stress–strain curves for NW, DW_{SD}, CDW_{SD0}, CDW_{SD9}, and CDW_{SD18}. The respective (b) tensile strength, (c) Young’s modulus, and (d) toughness from the tensile stress–strain curves.

Figure 4 shows the stress distributions of CDW_{SD0} (Figure 4a), CDW_{SD9} (Figure 4b), and CDW_{SD18} (Figure 4c) when subjected to tension load. Meanwhile, Videos S1–S3 (Supporting Information) also present the variations of stress distributions during the loading process. The results of macro FEA indicated that the main loading was located at the middle of the sample. The CDW_{SD18} possessed superior tensile strength (365.5 MPa) compared to CDW_{SD9} (302.2 MPa) and CDW_{SD0} (78.4 MPa), which was also in accordance with the experimental studies.

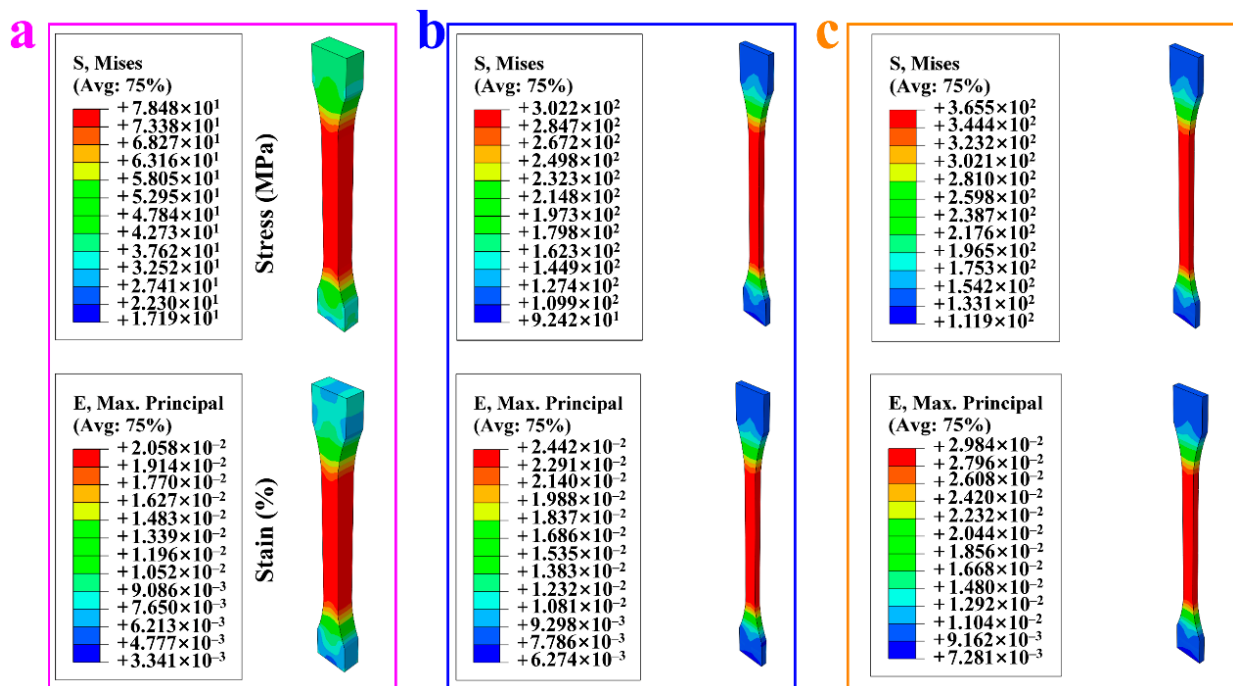


Figure 4. The macro finite element analysis of (a) CDW_{SD0}, (b) CDW_{SD9}, and (c) CDW_{SD18}.

Figure 5 presents the stress distributions of a representative bulk unit cell, cellulose nanofibril, and nanofibril mesenchyme models of CDW_{SD0} (Figure 5a), CDW_{SD9} (Figure 5b), and CDW_{SD18} (Figure 5c) during the micro FEA process. The micro FEA result indicated that the main breaking points belonged to cellulose nanofibril mesenchyme, which was consistent with experimental data. There are some burrs at the breaking point that also proved that the cellulose nanofibril mesenchyme, not cellulose nanofibril, experienced fracture in tensile testing. With the increase in moisture content in compressed samples, the tensile strength was gradually improved, which illustrated that the hydrogen bonding among cellulose nanofibrils was increased from the qualitative perspective. Therefore, the CDW can endure higher stress, which was caused by bigger fracture forces of cellulose nanofibril mesenchyme with the increase in moisture content.

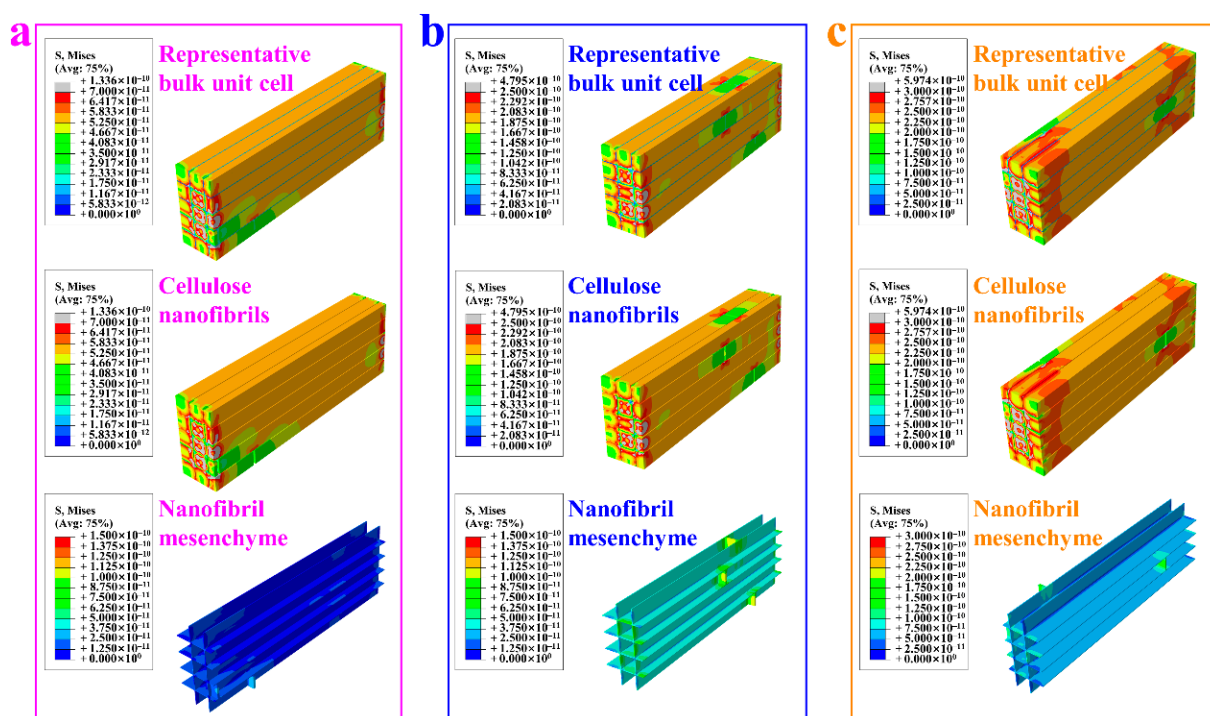


Figure 5. The stress distributions of representative bulk unit cell, cellulose nanofibrils, and nanofibril mesenchyme for (a) CDW_{SD0} , (b) CDW_{SD9} , and (c) CDW_{SD18} during micro finite element analysis process.

4. Conclusions

In this work, we reviewed a strong and tough material and investigated the dynamic tensile deformation behavior of this material by using macro/micro FEA and experimental methods. The deformation modes for compressed delignified wood under different moisture contents subjected to dynamic mechanical stretching were identified. The following conclusions were drawn: (1) the numerical simulation and theoretical analysis results were in accordance with experimental data; (2) FEA was an effective approach to predict the fracture position and force situation for samples under dynamic stress; (3) the results of FEA showed that water molecules can serve as plasticizers and hydrogen-bonding bridges to simultaneously enhance strength and toughness. In conclusion, the proposed macro/micro FEA is capable of being used to evaluate the dynamic mechanical properties and reveal strengthening mechanisms for cellulosic materials, which will contribute to fabricating superior structural composites.

Supplementary Materials: The following supporting information can be downloaded at: <https://www.mdpi.com/article/10.3390/polym14214490/s1>, Figure S1: Representative bulk unit cell models of (a) CDW_{SD0}, (b) CDW_{SD9}, and (c) CDW_{SD18}; Figure S2: The photograph of DW_{SD} and CDW_{SD18}; Video S1: The stress distribution variation of CDW_{SD0}; Video S2: The stress distribution variation of CDW_{SD9}; Video S3: The stress distribution variation of CDW_{SD18}.

Author Contributions: X.H.: Investigation, Conceptualization, Methodology, Writing—Original Draft Preparation. J.W.: Resources, Investigation. X.W.: Data curation. W.T.: Methodology, Validation. Y.D.: Conceptualization, Writing—Reviewing and Editing. S.J.: Writing—Reviewing and Editing, Supervision. All authors have read and agreed to the published version of the manuscript.

Funding: This research was funded by Foundation of State Key Laboratory of Biobased Material and Green Papermaking, Qilu University of Technology, Shandong Academy of Sciences (No. GZKF202129).

Institutional Review Board Statement: Not applicable.

Data Availability Statement: The data used to support the findings of this study are available from the corresponding author upon request.

Acknowledgments: We acknowledge the support of the Foundation of State Key Laboratory of Biobased Material and Green Papermaking, Qilu University of Technology, Shandong Academy of Sciences (No. GZKF202129).

Conflicts of Interest: The authors declare that they have no known competing financial interest or personal relationships that could have appeared to influence the work reported in this paper.

References

1. Xia, L.L.; Tu, H.J.; Zeng, W.; Yang, X.L.; Zhou, M.; Li, L.K.; Guo, X. A room-temperature self-healing elastomer with ultra-high strength and toughness fabricated via optimized hierarchical hydrogen-bonding interactions. *J. Mater. Chem. A* **2022**, *10*, 4344–4354. [[CrossRef](#)]
2. Duan, G.; Jin, M.; Wang, F.; Greiner, A.; Agarwal, S.; Jiang, S. Core effect on mechanical properties of one dimensional electrospun core-sheath composite fibers. *Compos. Commun.* **2021**, *25*, 100773. [[CrossRef](#)]
3. Zhou, X.; Ding, C.; Cheng, C.; Liu, S.; Duan, G.; Xu, W.; Liu, K.; Hou, H. Mechanical and thermal properties of electrospun polyimide/rGO composite nanofibers via in-situ polymerization and in-situ thermal conversion. *Eur. Polym. J.* **2020**, *141*, 110083. [[CrossRef](#)]
4. Williams, J.C.; Starke Jr, E.A. Progress in structural materials for aerospace systems. *Acta Mater.* **2003**, *51*, 5775–5799. [[CrossRef](#)]
5. Wu, G.; Sun, J.; Huang, C.; Ren, H.; Zhao, R. Research progress on mechanical properties of tenon-mortise joints in traditional Chinese wood structures. *J. For. Eng.* **2020**, *5*, 29–37.
6. Wang, D.; Yu, J.; Duan, G.; Liu, K.; Hou, H. Electrospun polyimide nonwovens with enhanced mechanical and thermal properties by addition of trace plasticizer. *J. Mater. Sci.* **2020**, *55*, 5667–5679. [[CrossRef](#)]
7. Lin, X.H.; Zhang, L.N.; Duan, B. Polyphenol-mediated chitin self-assembly for constructing a fully naturally resourced hydrogel with high strength and toughness. *Mater. Horiz.* **2021**, *8*, 2503–2512. [[CrossRef](#)]
8. Chen, L.; Cao, S.; Huang, L.; Wu, H.; Hu, H.; Liu, K.; Lin, S. Development of bamboo cellulose preparation and its functionalization. *J. For. Eng.* **2021**, *6*, 1–13.
9. Li, T.; Chen, C.J.; Brozena, A.H.; Zhu, J.Y.; Xu, L.X.; Driemeier, C.; Dai, J.Q.; Rojas, O.J.; Isogai, A.; Wagberg, L.; et al. Developing fibrillated cellulose as a sustainable technological material. *Nature* **2021**, *590*, 47–56. [[CrossRef](#)]
10. Moon, R.J.; Martini, A.; Nairn, J.; Simonsen, J.; Youngblood, J. Cellulose nanomaterials review: Structure, properties and nanocomposites. *Chem. Soc. Rev.* **2011**, *40*, 3941–3994. [[CrossRef](#)]
11. Han, X.S.; Ding, L.H.; Tian, Z.W.; Wu, W.J.; Jiang, S.H. Extraction and characterization of novel ultrastrong and tough natural cellulosic fiber bundles from manau rattan (*Calamus manan*). *Ind. Crops Prod.* **2021**, *173*, 114103. [[CrossRef](#)]
12. Han, X.S.; Wang, J.B.; Wang, J.W.; Ding, L.H.; Zhang, K.; Han, J.Q.; Jiang, S.H. Micro- and nano-fibrils of manau rattan and solvent-exchange-induced high-haze transparent holocellulose nanofibril film. *Carbohydr. Polym.* **2022**, *298*, 120075. [[CrossRef](#)] [[PubMed](#)]
13. Cai, S.; Li, Y.; Huang, Y.; Guo, Y. Study on correlation between mechanical measurement of wood cell wall and added load by nano-indentation. *J. For. Eng.* **2021**, *6*, 64–71.
14. Ji, F.; Sun, Z.; Hang, T.; Zheng, J.; Li, X.; Duan, G.; Zhang, C.; Chen, Y. Flexible piezoresistive pressure sensors based on nanocellulose aerogels for human motion monitoring: A review. *Compos. Commun.* **2022**, *35*, 101351. [[CrossRef](#)]
15. Dufresne, A. *Nanocellulose: From Nature to High Performance Tailored Materials*; Walter de Gruyter GmbH & Co KG: Berlin, Germany, 2017.
16. Sturcova, A.; Davies, G.R.; Eichhorn, S.J. Elastic modulus and stress-transfer properties of tunicate cellulose whiskers. *Biomacromolecules* **2005**, *6*, 1055–1061. [[CrossRef](#)]

17. Zhu, H.L.; Zhu, S.Z.; Jia, Z.; Parvinian, S.; Li, Y.Y.; Vaaland, O.; Hu, L.B.; Li, T. Anomalous scaling law of strength and toughness of cellulose nanopaper. *Proc. Natl. Acad. Sci. USA* **2015**, *112*, 8971–8976. [[CrossRef](#)]
18. Li, K.; Skolrood, L.N.; Aytug, T.; Tekinalp, H.; Ozcan, S. Strong and Tough Cellulose Nanofibrils Composite Films: Mechanism of Synergetic Effect of Hydrogen Bonds and Ionic Interactions. *ACS Sustain. Chem. Eng.* **2019**, *7*, 14341–14346. [[CrossRef](#)]
19. Song, J.W.; Chen, C.J.; Zhu, S.Z.; Zhu, M.W.; Dai, J.Q.; Ray, U.; Li, Y.J.; Kuang, Y.D.; Li, Y.F.; Quispe, N.; et al. Processing bulk natural wood into a high-performance structural material. *Nature* **2018**, *554*, 224–228. [[CrossRef](#)]
20. Wang, Q.Q.; Yao, Q.; Liu, J.; Sun, J.Z.; Zhu, Q.Q.; Chen, H.L. Processing nanocellulose to bulk materials: A review. *Cellulose* **2019**, *26*, 7585–7617. [[CrossRef](#)]
21. Zhao, K.X.; Wang, W.H.; Teng, A.G.; Zhang, K.; Ma, Y.H.; Duan, S.M.; Li, S.Z.; Guo, Y. Using cellulose nanofibers to reinforce polysaccharide films: Blending vs layer-by-layer casting. *Carbohydr. Polym.* **2020**, *227*, 115264. [[CrossRef](#)]
22. Xiao, J.; Li, H.; Zhang, H.; He, S.; Zhang, Q.; Liu, K.; Jiang, S.; Duan, G.; Zhang, K. Nanocellulose and its derived composite electrodes toward supercapacitors: Fabrication, properties, and challenges. *J. Bioresour. Bioprod.* **2022**. [[CrossRef](#)]
23. Benitez, A.J.; Walther, A. Counterion Size and Nature Control Structural and Mechanical Response in Cellulose Nanofibril Nanopapers. *Biomacromolecules* **2017**, *18*, 1642–1653. [[CrossRef](#)] [[PubMed](#)]
24. Benitez, A.J.; Walther, A. Cellulose nanofibril nanopapers and bioinspired nanocomposites: A review to understand the mechanical property space. *J. Mater. Chem. A* **2017**, *5*, 16003–16024. [[CrossRef](#)]
25. Huang, D.; Li, D.; Mo, K.W.; Xu, R.; Huang, Y.A.; Cui, Y.D.; Zhang, Q.C.; Chang, C.Y. Top-down fabrication of biodegradable multilayer tunicate cellulose films with controlled mechanical properties. *Cellulose* **2021**, *28*, 10415–10424. [[CrossRef](#)]
26. Garemark, J.; Yang, X.; Sheng, X.; Cheung, O.; Sun, L.C.; Berglund, L.A.; Li, Y.Y. Top-Down Approach Making Anisotropic Cellulose Aerogels as Universal Substrates for Multifunctionalization. *ACS Nano* **2020**, *14*, 7111–7120. [[CrossRef](#)] [[PubMed](#)]
27. Zhu, M.W.; Jia, C.; Wang, Y.L.; Fang, Z.Q.; Dai, J.Q.; Xu, L.S.; Huang, D.F.; Wu, J.Y.; Li, Y.F.; Song, J.W.; et al. Isotropic Paper Directly from Anisotropic Wood: Top-Down Green Transparent Substrate Toward Biodegradable Electronics. *ACS Appl. Mater. Interfaces* **2018**, *10*, 28566–28571. [[CrossRef](#)] [[PubMed](#)]
28. Zou, Y.; Zhao, J.; Zhu, J.; Guo, X.; Chen, P.; Duan, G.; Liu, X.; Li, Y. A Mussel-Inspired Polydopamine-Filled Cellulose Aerogel for Solar-Enabled Water Remediation. *ACS Appl. Mater. Interfaces* **2021**, *13*, 7617–7624. [[CrossRef](#)]
29. Li, T.; Zhai, Y.; He, S.M.; Gan, W.T.; Wei, Z.Y.; Heidarinejad, M.; Dalgo, D.; Mi, R.Y.; Zhao, X.P.; Song, J.W.; et al. A radiative cooling structural material. *Science* **2019**, *364*, 760–763. [[CrossRef](#)]
30. Zhu, M.W.; Wang, Y.L.; Zhu, S.Z.; Xu, L.S.; Jia, C.; Dai, J.Q.; Song, J.W.; Yao, Y.G.; Wang, Y.B.; Li, Y.F.; et al. Anisotropic, Transparent Films with Aligned Cellulose Nanofibers. *Adv. Mater.* **2017**, *29*, 1606284. [[CrossRef](#)]
31. Neves, R.M.; Ornaghi, H.L.; Zattera, A.J.; Amico, S.C. Recent studies on modified cellulose/nanocellulose epoxy composites: A systematic review. *Carbohydr. Polym.* **2021**, *255*, 117366. [[CrossRef](#)]
32. Chen, Q.H.; Jiang, Z.Y.; Pei, X.X.; Liu, Y.Q.; Du, R.K.; Zhao, G.Z. Bio-inspired, epoxy-based lamellar composites with superior fracture toughness by delignified wood scaffold. *Compos. Sci. Technol.* **2021**, *207*, 108739. [[CrossRef](#)]
33. Kuai, B.B.; Wang, Z.H.; Gao, J.S.; Tong, J.W.; Zhan, T.Y.; Zhang, Y.L.; Lu, J.X.; Cai, L.P. Development of densified wood with high strength and excellent dimensional stability by impregnating delignified poplar by sodium silicate. *Constr. Build. Mater.* **2022**, *344*, 128282. [[CrossRef](#)]
34. Han, X.S.; Ye, Y.H.; Lam, F.; Pu, J.W.; Jiang, F. Hydrogen-bonding-induced assembly of aligned cellulose nanofibers into ultrastrong and tough bulk materials. *J. Mater. Chem. A* **2019**, *7*, 27023–27031. [[CrossRef](#)]
35. Hu, W.G.; Chen, B.R.; Zhang, T.X. Experimental and numerical studies on mechanical behaviors of beech wood under compressive and tensile states. *Wood Res.* **2021**, *66*, 27–37. [[CrossRef](#)]
36. Valachova, D.; Skotnicova, I. Using the finite element method to predict heat dissipation in a timber frame building construction. *Wood Res.* **2019**, *64*, 859–870.
37. Hu, W.G.; Chen, B.R. A Methodology for Optimizing Tenon Geometry Dimensions of Mortise-and-Tenon Joint Wood Products. *Forests* **2021**, *12*, 478. [[CrossRef](#)]
38. Hu, W.G.; Wan, H.; Guan, H.Y. Size Effect on the Elastic Mechanical Properties of Beech and Its Application in Finite Element Analysis of Wood Structures. *Forests* **2019**, *10*, 783. [[CrossRef](#)]
39. Sluiter, A.; Hames, B.; Ruiz, R.; Scarlata, C.; Sluiter, J.; Templeton, D.; Crocker, D.; Templeton, D. Determination of structural carbohydrates and lignin in biomass. *Lab. Anal. Proced.* **2008**, *1617*, 1–16.
40. Klemm, D.; Kramer, F.; Moritz, S.; Lindstrom, T.; Ankerfors, M.; Gray, D.; Dorris, A. Nanocelluloses: A New Family of Nature-Based Materials. *Angew. Chem. Int. Ed.* **2011**, *50*, 5438–5466. [[CrossRef](#)]